Met. Mater. Int., Vol. 20, No. 3 (2014), pp. 445~450
doi: 10.1007/s12540-014-3007-4

Finite Element Analysis of the Effect of Friction in High Pressure Torsion

Yuepeng Song[1,2,3,*], Wenke Wang[1], Dongsheng Gao[3], Eun Yoo Yoon[4], Dong Jun Lee[2], and Hyoung Seop Kim[2,*]

[1]Shandong Agricultural University, Mechanical and Electronic Engineering College, Tai'an 271018, China
[2]Pohang University of Science and Technology, Department of Materials Science and Engineering, Pohang 790-784, Korea
[3]Shandong Agricultural University, Shandong Provincial Key Laboratory of Horticultural Machineries and Equipments, Tai'an, China
[4]Korea Institute of Materials Science, Materials Deformation Department, Changwon 641-831, Korea

(received date: 1 December 2012 / accepted date: 28 September 2013)

High pressure torsion (HPT) is one of the most important techniques among various methods that create severe plastic deformation in the production of bulk materials with nano/ultrafine grained microstructures. Since the driving force in deforming the workpiece in HPT is surface friction, understanding of the friction effect is critical for successful application of HPT. In this study, the friction effect in HPT was analyzed using the finite element method. The distribution of effective strain on the contact surface of the HPT samples under different friction conditions was investigated. The friction force influenced the effective strain more in the middle and edge regions than in the central region. The condition for the minimum friction factor that could achieve a sticking condition between the surfaces of the dies, and the samples in the middle and edge regions, was investigated. There was a critical friction coefficient in which the effective strain varies sharply with an increasing friction coefficient.

Key words: severe plastic deformation, plasticity, work hardening, finite element method, grain size

1. INTRODUCTION

The number of investigations on the microstructural evolution of ultrafine-grained (UFG) materials surged tremendously during the last 20 years because UFG materials exhibit outstanding characteristics, especially mechanical properties [1-4]. Utilization of severe plastic deformation (SPD) methods has provided a convenient approach for producing bulk metallic UFG materials [5-13]. Several SPD methods have been proposed, such as equal-channel angular pressing, high-pressure torsion (HPT), accumulated roll bonding, and cyclic extraction compression. To date, the HPT process has proven to be the most effective of all the SPD methods in producing bulk, nanostructured materials with exceptionally small grain sizes [14-19].

The principle of the HPT process is that a sample, generally in the form of a thin disk, is subjected to high pressure between massive anvils and then processed through the application of torsional straining. One die is turned at a given rotation speed and surface frictional forces deform the sample by shearing so that deformation proceeds under a quasi-hydrostatic state. Thus, the friction between the sample and the die plays an important role in the deformation of the sample. Indeed, the mechanical properties that result from the interface between the two materials, and the friction between the die and the work piece, are critical in many metal forming processes [20-25]. The HPT process consists of two stages (compression and torsion) based on the motion of the lower dies and the samples, as shown in Fig. 1. During the torsion stage, the compressive pressure is generally kept constant. The high imposed-compressive-hydrostatic pressure prevents cracking of the sample inside the die and the low thickness-to-diameter ratio results in the production of a high strain during the die rotation. In practice, the effective strain 'ε' imposed on the sample may be defined as:

$$\varepsilon = \frac{2\pi NR}{h\sqrt{3}} \tag{1}$$

where N is the number of turns in the HPT, R is the distance from the center of the sample, and h is the sample thickness [26-28].

*Corresponding author: ustbsong@sina.com, hskim@postech.ac.kr

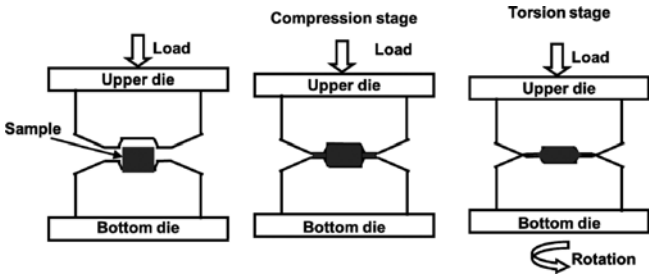

Fig. 1. Schematic diagram of high pressure torsion processing (compression stage and torsion stage).

The HPT process involves changing the shape of the sample by forcing it to flow through a system which requires tight contact between the die and sample. As a result of this contact, tangential frictional forces are generated at the interface of the die/sample that resist this relative movement. It is known that frictional conditions at the interface of the die/sample can affect the metal flow, finial properties of the sample, total deformation load, and premature die wear. The effect of friction between the sample and the dies is complex and results in the appearance of surface shear, particularly in HPT. Thus, friction is considered to be a major variable in metal forming processes where the sample undergoes large plastic deformations [29].

Although many studies have been done on HPT, most of them have been on microstructure and its characterization, or on processing. Because the mechanical properties of the deformed material are directly related to the effect of friction, understanding this effect is very important for successful application of the HPT process. This paper presents the results of a finite element analysis of the effect of friction during the HPT process. Simulation of the distribution of effective strain on the contact surface of the HPT samples was carried out using the commercial rigid/plastic finite element code, DEFORM [30,31].

2. CALCULATION PROCEDURES

Simulations of plastic deformation during the HPT process were performed using the commercial rigid/plastic finite element code, DEFORM. The geometries of the dies and the sample used in this study are shown in Fig. 2; it should be noted that the sizes of the samples were identical to those described in a recent report on HPT [29]. The disk in the recent report had an initial thickness of 2.0 mm and a diameter of 19.5 mm, as shown in Fig. 2, and the two dies had a shallow central depression on their outer surfaces [32,33].

The number of initial meshes in the sample was 25,521 and this number of elements was enough to show the local deformation of the sample by calculation. A force was applied to the upper die to move it towards the bottom die. This force was calculated to provide pressure of 10.0 GPa on the initial

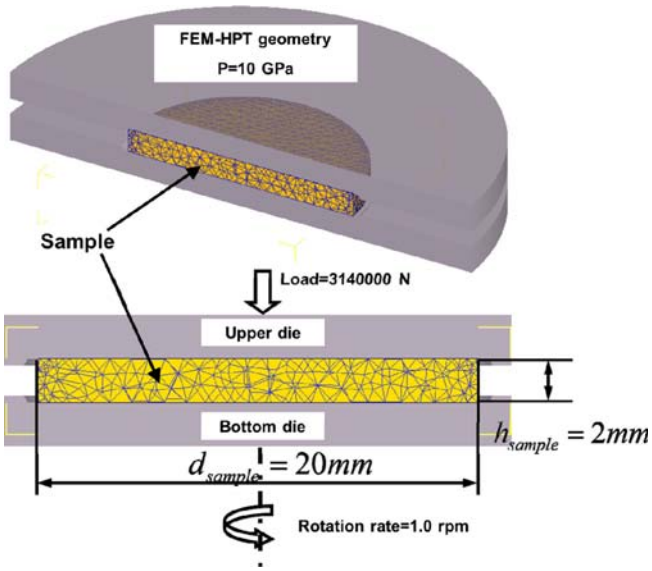

Fig. 2. Illustration of the geometry of the dies and details of the geometry of the sample used in the simulation of quasi-constrained HPT processing.

contact area of the sample. The friction factors between the dies and sample were assumed to be 0.5, 0.7, 0.9, 1.0, 1.5, and 2.0, respectively. The revolutions applied to the bottom die were 0, 1/4, 2/4, 3/4, and 1 turns. The standard simulation, with pressure of 10.0 GPa and rotation rate of 1.0 rpm (Fig. 2), was used for comparison with other simulations having different input parameters. The durations of the compression and torsion stages were all set at 10 s.

3. RESULTS AND DISCUSSION

Figure 3 shows the evolution in effective strain at the selected point in the middle of the HPT sample for the friction coeffi-

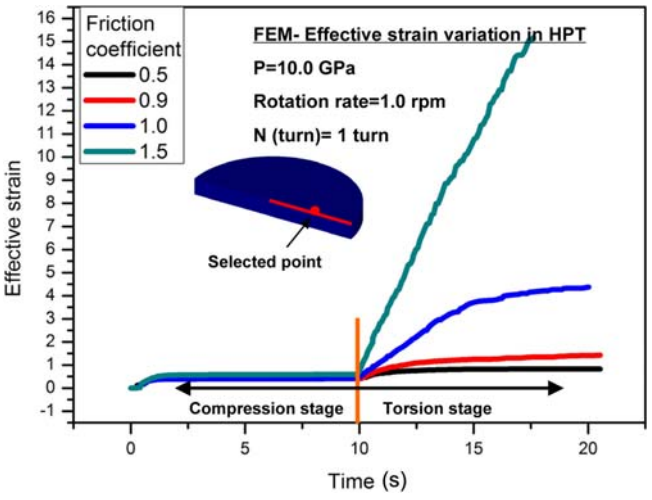

Fig. 3. Simulated evolution in strain with the variation of the friction coefficient at the selected point in the medium of the HPT samples.

cients 0.5, 0.9, 1.0 and 1.5. The pressure was fixed at 10 GPa and the number of turns was 1. Several important conclusions can be drawn from inspection of Fig. 3. First, the effective strain values are almost the same in the compression stage at a constant of 0.4-0.6, which means that the friction had no effect on the evolution of effective stain on the contact surface of the HPT samples. By contrast, the effective strain is expected to increase due to the increase of the friction coefficient between the samples and the dies in the torsion stage. That is to say, the friction plays an important role on the evolution of effective strain in the torsion stage.

Another important factor is that the effective strain will reach quasi-saturation at the saturated effective strain values of 0.82, 1.33, and 4.17; when the friction coefficients are 0.5, 0.9, and 1.0, respectively. Meanwhile, the times to reach strain saturation also differ with the variation of the friction coefficient; thus, the strain saturating times are 12.1, 13.4, and 19.0 s when the friction coefficients are 0.5, 0.9 and 1.0, respectively, as shown in Fig. 3. However, it should also be stressed that the effective strain cannot reach quasi-saturation at the friction coefficient of 1.5 in 20 s. Since the friction drives the surface of the sample to rotate, the effective strain increases remarkably with an increasing number of the revolutions in the torsion stage, compared to strains in the compression stage. These results suggest that the friction between the sample and the die directly affects the planes of principal stress, and therefore is a major factor in the HPT process during which the samples undergo large plastic deformation.

The simulations were performed for the friction coefficients of 0.5, 0.7, 0.9, 1.0, 1.5, and 2.0 between the sample and the die to investigate the strain distribution on the contact surface of the HPT samples with different friction coefficients, see Fig. 4a. Although the effective-strain values in the central region were similar under different friction coefficients, the variations of effective strain according to the distance from the center were different under low (<0.9) and high (>1.0) friction coefficients. The effective strain values changed little along the distance from the center when the friction coefficients were 0.5, 0.7, and 0.9. However, the strain values increased significantly with increasing distance from the center when the friction coefficients were 1, 1.5, and 2. The friction force affected the effective strain more in the middle and edge regions than in the central region. The different effective strain distributions, according to the distance from the center at different friction coefficients, were due to the friction-shear stress. In the middle and edge regions, the friction-shear stress based on a high friction coefficient was high enough to achieve a sticking condition between the surfaces of the dies and samples. Figure 4 clearly indicates lower values of effective strain in the central region and high values in the edge region, particularly at higher friction coefficients. Since the frictional-shear stress (normal stress x friction coefficient, i.e., the frictional force per area) and normal stress distributions on the contact surface are non-uniform [34], the non-uniform effective strain is attributed to the non-uniform frictional-shear stress (i.e., the non-uniform normal stress).

The variation of effective strain according to different positioning of the work piece, with increasing friction coefficient, was further investigated (Fig. 4b). The figure clearly indicates that there exist two key points of increasing friction coefficient (0.9 and 1.5). Within this range of friction coefficient (from 0.9 to 1.5), the effective strain sharply increased, particularly in the middle and edge areas. However, outside this range of friction coefficient (<0.9 or >1.5), the effective strain varied constantly. That is to say, there is a critical friction coefficient value at which the effective strain increases sharply, which also agrees very well with the former conclusion.

Figure 5 shows the values of the effective strain across the diameter of the samples processed by HPT at the friction coefficients of (a) 0.5, (b) 1.0, and (c) 1.5; with different num-

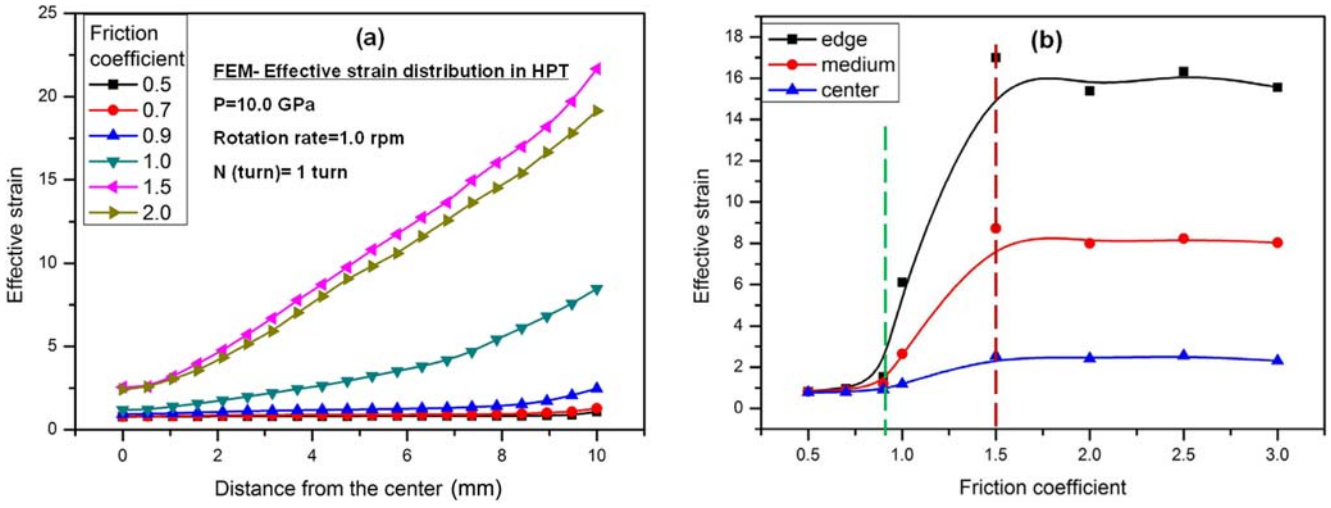

Fig. 4. Simulated effective strain distribution on the contact surface of the HPT samples along with the different friction coefficient.

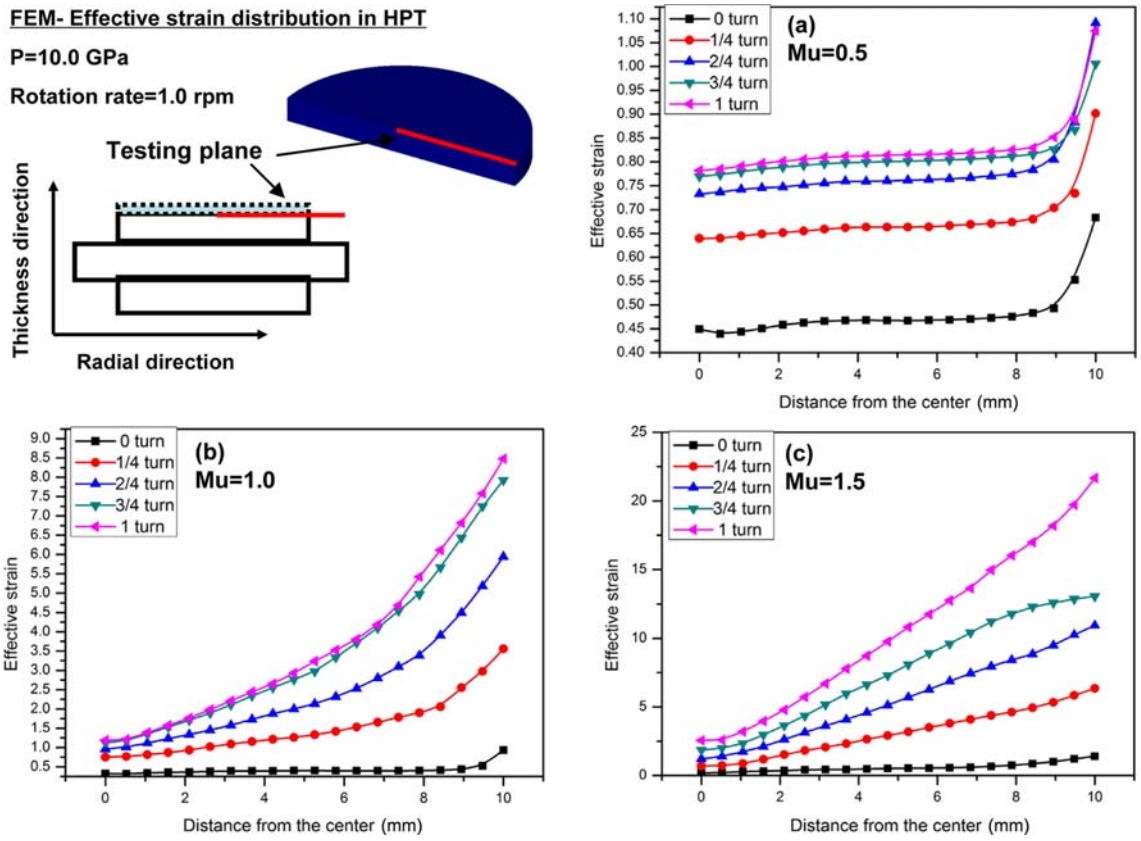

Fig. 5. Effective strain distribution of the HPT samples after various turns with (a) the friction coefficient of 0.5, (b) the friction coefficient of 1.0, and (c) the friction coefficient of 1.5.

bers of turns. The effective strain of the sample was uniform in the central and middle regions, when the friction coefficient was 0.5, as can be seen in Fig. 5a. The effective strain increased as the friction coefficient increased with an almost linear relationship when the friction coefficient was 1.5 as in Fig. 5c. According to Eq. 1, the torsion strain changes linearly from zero at the center of the sample to the maximum value at the edge. These results suggest that the friction force (i.e., the friction coefficient) will influence the effective strain more in the middle and edge regions than in the central region. The difference in the trend of effective strain under different friction coefficients, particularly in the middle and edge regions, may be attributed to the friction-shear stress, which is high enough to achieve a sticking condition between the surfaces of the dies and the samples due to the higher friction coefficient.

It should be noted that this friction-shear stress will play a more important role in the deformation behavior of the material in the torsion stage than in the compression stage, as can be seen in Fig. 5. The effective strains changed little after 2/4 turns and 3/4 turns, when the friction coefficients were 0.5 and 1.0, respectively. In particular, the effective strain value increased steadily when the friction coefficient was 1.5. This situation corresponds to the results in Fig. 3, in which the effective strain reached quasi-saturation as the number of

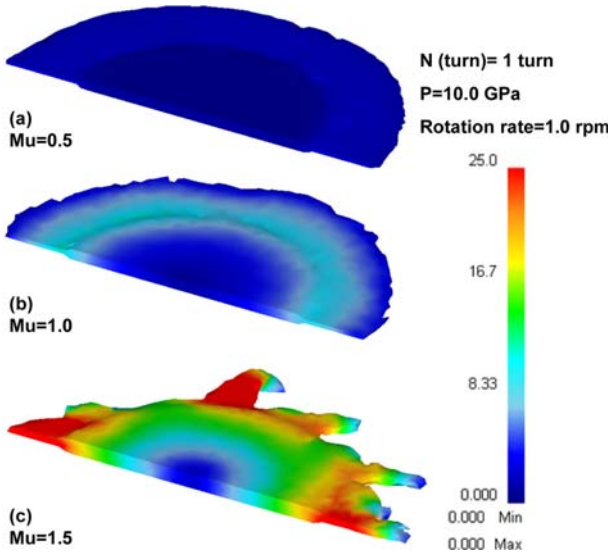

Fig. 6. FEM predication of the effective strain distribution of the samples with (a) the friction coefficient of 0.5, (b) the friction coefficient of 1.0 and (c) the friction coefficient of 1.5.

revolutions increased in the torsion stage. These results can be attributed to the frictional stress, which forces the surface of the samples to rotate in the torsion stage, below the range

of critical friction coefficients.

The effective-strain distributions of the samples processed by HPT under different friction coefficients are shown in Fig. 6 at the applied pressure of 10.0 GPa, rotation speed of 1.0 rpm, and number of turns of 1. The values of the effective strain in the edge region were 1.1, 9.0, and 18.4 under the friction coefficients of 0.5, 1.0, and 1.5, respectively (Fig. 6). Meanwhile, Fig. 6 clearly indicates a low effective strain in the center and high values on the edge, demonstrating that the effective strain proceeds gradually from the edge to the center. Interestingly, Fig. 6c indicates that when the friction coefficient was 1.5, the friction between the flash of the sample and the dies was so huge that the flash region tore. These results of effective strain distribution may be attributed to two causes: (1) the huge friction between the flash region and dies restricts the metal flow and the friction shear stress is high enough to achieve a sticking condition between the surfaces of the dies and the sample, and (2) torsional deformation without any compression induces higher strain in the outer region, i.e., friction-shear strain is proportional to the radius and zero at the center, according to classical torsion theory.

4. CONCLUSIONS

In this paper, the results of finite element analysis of the effect of friction in HPT were presented. The distribution of the effective strain on the contact surface of the HPT samples under different friction coefficients was investigated. Friction played a more important role in the evolution of effective strain in the torsion stage than in the compression stage, and the friction force influenced the effective strain more in the middle and edge regions than in the central region. We determined that a high friction coefficient was enough to achieve a sticking condition between the surfaces of the dies and the samples in the medium and edge regions. We also found that there is a critical friction coefficient in which the effective strain varies sharply with increasing friction coefficient. Analysis by the finite element method for the HPT process is useful if the material parameters are incorporated. Further local and non-local investigations are necessary.

ACKNOWLEDGMENTS

Y. P. Song acknowledges the postdoctoral fellowship supported by the National Research Foundation through the Korea-China Young Scientists Program, Korea. Furthermore, this work was also supported by Key Laboratory of Functional Crystals and Laser Technology, TIPC, CAS. Chinese National Fusion Project for ITER (NO. 2013GB110005), China Postdoctoral Science Foundation (2013M531636), Shandong Postdoctoral Innovative program (201203101), Special project for independent innovation of Shandong province (2013CXC90201), Special fund of modern agricultural technology system of Shandong Province-Fruit innovation team (SPAIT-03-022-05). This study was supported by a grant from the Fundamental R&D Program for Core Technology of Materials (100372751-55551) funded by the Ministry of Knowledge Economy, Korea.

REFERENCES

1. Z. Xie, J. Xie, Y. Hong, and X. Wu, *Sci. China Tech. Sci.* **53**, 1534 (2010).
2. H. S. Kim, Y. Estrin and M. B. Bush, *Acta Mater.* **48**,493 (2000).
3. H. S. Kim and Y. Estrin, *Appl. Phys. Lett.* **79**, 4115 (2001).
4. H. S. Kim, C. Suryanarayana, and S. J. Kim, *Powder Metall.* **41**, 217 (1998).
5. R. Z. Valiev and T. G. Langdon, *Prog. Mater. Sci.* **51**, 881 (2006).
6. B. Hadzima, M. Janeèek, Y. Estrin, and H. S. Kim, *Mater. Sci. Eng. A* **462**, 243 (2007).
7. M. Vaseghi, A. K. Taheri, and H. S. Kim, *Met. Mater. Int.* **16**, 363 (2010).
8. G. Purcek, O. Saray, and O. Kul, *Met. Mater. Int.* **16**, 145 (2010).
9. S. C. Yoon, A. V. Nagasekhar, and H. S. Kim, *Met. Mater. Int.* **15**, 215 (2009).
10. H. S. Kim. M. H. Seo, and S. I. Hong, *Mater. Sci. Eng. A* **291**, 86 (2000).
11. H. S. Kim and Y. Estrin, *Mater. Sci. Eng. A* **410**, 285 (2005).
12. S.-H. Lee and J.-H. Kim, *Korean J. Met. Mater.* **51**, 41 (2013).
13. K. H. Lee and S. I. Hong, *Korean J. Met. Mater.* **51**, 621 (2013).
14. C. Xu, Z. Horita, and T. G. Langdon, *Acta Mater.* **56**, 5168 (2008).
15. A. P. Zhilyaev, K. Oh-ishi, T. G. Langdon, and T. R. McNelley, *Mater. Sci. Eng. A* **410**, 277 (2005).
16. L. Kurmanaeva, Y. Ivanisenko, J. Markmann, C. Kübel, A. Chuvilin, S. Doyle, R. Z. Valiev, and H. J. Fecht, *Mater. Sci. Eng. A* **527**, 1776 (2010).
17. A. P. Zhilyaev and T. G. Langdon, *Prog. Mater. Sci.* **53**, 893 (2008).
18. E. Y. Yoon, D. J. Lee, B. H. Park, M. R. Akbarpour, M. Farvizi, and H. S. Kim, *Met. Mater. Int.* **19**, 927 (2013).
19. W. Wang, Y. Song, D. Gao, E. Y. Yoon, D. J. Lee, C. S. Lee, and H. S. Kim, *Met. Mater. Int.* **19**, 1021 (2013).
20. E.-Y. Kim, J.-H. Cho, H.-W. Kim, and S.-H. Choi, *Korean J. Met. Mater.* **51**, 41 (2013).
21. S. Lee, J.-S. Lee, Y.-B. Kim, G.-A. Lee, S.-P. Lee, I.-S. Son, J.-K. Lee, and D.-S. Bae, *Korean J. Met. Mater.* **51**, 655 (2013).
22. E. K. Lee and S. I. Hong, *Korean J. Met. Mater.* **51**, 15 (2013).
23. J. K. Lim, S. Y. Choi, K. H. Choe, S. S. Kim, and G. S. Cho, *Korean J. Met. Mater.* **51**, 385 (2013).
24. K. S. Lee, S. E. Lee, J. S. Kim, M. J. Kim, D. H. Bae, and Y. N. Kwon, *Korean J. Met. Mater.* **51**, 535 (2013).

25. J. S. Kim, K. S. Lee, Y. N. Kwon, Y. S. Lee, S. Lee, and Y. W. Chang, *Korean J. Met. Mater.* **51**, 547 (2013).
26. R. Z. Valiev, Y. V. Lvanisenko, E. F. Rauch, and B. Baudelet, *Acta Mater.* **44**, 4705 (1996).
27. F. Wetscher, A. Vorhauer, R. Stock, and R. Pippan, *Mater. Sci. Eng. A* **387**, 809 (2004).
28. F. Wetshcer, R. Pippan, S. Sturm, F. Kauffmann, and C. Scheu, *Metall. Mater. Trans. A* **37**, 1963 (2006).
29. Y. Song, E. Y. Yoon, D. J. Lee, J. H. Lee, and H. S. Kim, *Mater. Sci. Eng. A* **528**, 4840 (2011).
30. S. Y. Kang and B. Ko, *Korean J. Met. Mater.* **51**, 651 (2013).
31. S. C. Yoon, Z. Horita, and H. S. Kim, *J. Mater. Proc. Tech.* **201**, 32 (2008).
32. R. B. Figueiredo, P. H. R. Pereira, M. T. P. Aguilar, P. R. Cetlin, and T. G. Langdon, *Acta Mater.* **60**, 3190 (2012).
33. S. C. Yoon, Z. Horita, and H. S. Kim, *J. Mater. Proc. Tech.* **201**, 32 (2008).
34. H. S. Kim, *J. Mater. Proc. Tech.* **113**, 617 (2001).